Fowler–Nordheim Tunneling Induced Charge Transfer Plasmons between Nearly Touching Nanoparticles

Lin Wu,[†] Huigao Duan,[‡] Ping Bai,[†,*] Michel Bosman,[‡] Joel K. W. Yang,[‡] and Erping Li[†,§]

[†]Institute of High Performance Computing, A*STAR (Agency for Science, Technology and Research), 1 Fusionopolis Way, no. 16-16 Connexis North, Singapore 138632, [‡]Institute of Materials Research and Engineering, A*STAR (Agency for Science, Technology and Research), 3 Research Link, Singapore 117602, and [§]Department of Information Science & Electronic Engineering, Zhejiang University, Hangzhou 310058, China

ABSTRACT Reducing the gap between two metal nanoparticles down to atomic dimensions uncovers novel plasmon resonant modes. Of particular interest is a mode known as the charge transfer plasmon (CTP). This mode has been experimentally observed in touching nanoparticles, where charges can shuttle between the nanoparticles *via* a conductive path. However, the CTP mode for nearly touching nanoparticles has only been predicted theoretically to occur *via* direct tunneling when the gap is reduced to ~0.4 nm. Because of challenges in fabricating and characterizing gaps at these dimensions, experiments have been unable to provide evidence for this plasmon mode that is supported by tunneling. In this work, we consider an alternative tunneling process, that is, the well-known Fowler–Nordheim (FN) tunneling that occurs at high electric fields, and apply it for the first time in the theoretical investigation of plasmon resonances between nearly touching nanoparticles. This new approach relaxes the requirements on gap dimensions, and intuitively suggests that with a sufficiently high-intensity irradiation, the CTP can be excited *via* FN tunneling for a range of subnanometer gaps. The unique feature of FN tunneling induced CTP is the ability to turn on and off the charge transfer by varying the intensity of an external light source, and this could inspire the development of novel quantum devices.

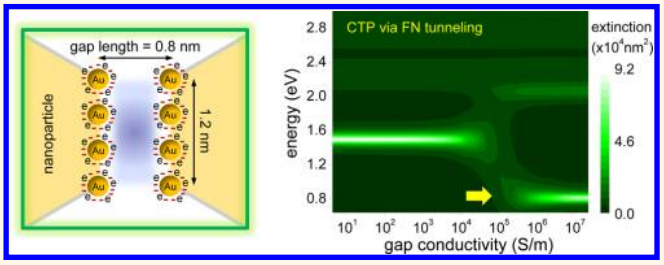

KEYWORDS: quantum plasmonics · charge transfer plasmons · nearly touching nanoparticles · direct tunneling · Fowler–Nordheim tunneling

Particle plasmon resonances occurring due to charge transfer across deep subnanometer gaps have been theoretically predicted[1−5] but have yet to be demonstrated experimentally. Despite a few attempts to observe charge transfer *via* tunneling in experiments,[6−9] this resonant mode remains elusive, even for the case of 0.5 nm gaps between pairs of nanoprisms.[8] Very recently, the effects of quantum tunneling on other higher-order plasmonic resonances are shown, though experimental evidence of the lowest-order charge transfer mode still remains elusive.[9] In existing theoretical treatments, quantum mechanical approaches have been applied to correctly model plasmon resonances of nanostructures with different gap dimensions. For very small gaps less than 0.4 nm, enough electrons can directly tunnel through the flat energy barrier between the nanoparticles and thus enable a charge transfer plasmon (CTP).[3−5] This type of direct tunneling dominates with decreasing gap size.[10] Thus far, these models have not considered Fowler–Nordheim tunneling, which is a field-emission effect in the presence of high electric fields.[11−14] This strong field effect has recently been alluded to in the full quantum mechanical study of the nonlinear effects for the field enhancement of a small nanoparticle dimer with sphere radius of ~2.17 nm (consisting of a few thousand conduction electrons).[4] Here, we focus on utilizing the strong field effect to achieve charge transfer plasmons between nearly touching nanoparticles with size on the order of a few tens of nanometers. To describe this typical plasmonic system used in experiments (consisting of millions or even billions conduction electrons), we will present a simplified quantum mechanical simulation model to cover the Fowler–Nordheim tunneling as well as the direct tunneling.

In the Fowler–Nordheim tunneling regime, the tunneling barrier between the nearly touching nanoparticles has a sloped

* Address correspondence to baiping@ihpc.a-star.edu.sg.

Received for review October 25, 2012 and accepted December 5, 2012.

Published online 10.1021/nn304970v

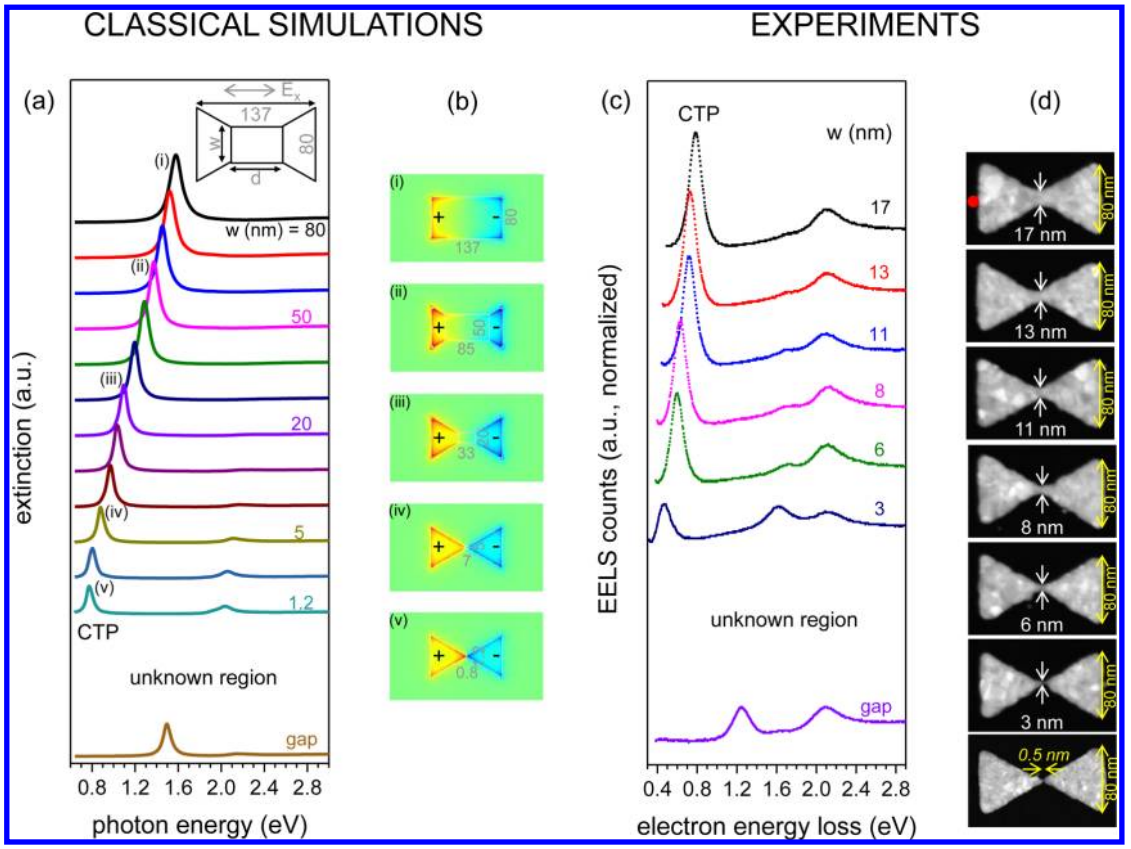

Figure 1. Systematic studies (including classical simulations and experiments) on charge transfer plasmons (CTPs) by continuously shrinking the size of the charge transfer path (width *w* and length *d*) within a 137-nm-long and 80-nm-wide single nanoparticle. (a) The simulated extinction spectra (assuming incident light polarized along the longitudinal axis) with different path sizes. The inset is the schematic of the simulated structure. (b) The simulated charge distributions for five representative path sizes at their respective resonant energies. (c) Experimental EELS spectra for different bridge widths. (d) HAADF STEM images of the fabricated structures on which EELS was performed. The location of the electron beam during the EELS experiments is indicated by the red dot. The slight shift of the measured CTP mode's resonant energies from the predicted energies by simulations could be due to the size mismatch between the fabricated and simulated structures.

energy-space profile. The electrons do not tunnel directly to the other nanoparticle. Instead, they can be thought to tunnel from the conduction band of one nanoparticle into the gap, from which they are swept into the other nanoparticle. Consequently, a conductive gap, or a "space charge" region, is formed.[15] In this context, we refer to the space charge as the continuum of electrons emitted from the surface of one nanoparticle and distributed over the entire gap region between the two nanoparticles. Owing to the formation of this conductive space charge region, the CTP—otherwise only present between touching nanoparticles—would then appear between nearly touching nanoparticles.[16] To the best of our knowledge, this is the first study focused on the charge transfer plasmons *via* Fowler–Nordheim tunneling.

In the present work, we will study the fundamentals of charge transfer between two nearly touching metal nanoprisms. In particular, we will focus on charge transfer plasmons (CTPs), where the conductive path to support CTPs will be the space charge or the emitted electrons in the gap.[15] We refer to this type of CTP as charge transfer plasmon *via* Fowler–Nordheim tunneling, and target to fully understand the fundamentals, including its physical origins, excitation mechanisms, characteristics such as the resonant energies, peak amplitudes, quality factors, as well as the key influential parameters such as the gap conductivity. To achieve these objectives, we combine quantum mechanical calculations (WKB-type approximation to solve the tunneling problem)[12–14] with classical electromagnetic optical simulations.

RESULTS AND DISCUSSION

Charge Transfer *via* a Conductive Bridge. We start our discussion with the plasmon resonance of a single rectangular nanoparticle. We show that the charge transfer plasmon (CTP) as supported by a conductive bridge can be viewed as a naturally evolved longitudinal dipolar plasmon mode of a single nanoparticle, where a neck is gradually formed. As shown by the classical electromagnetic calculations (with incident light polarized along the longitudinal axis) in Figure 1a and 1b, a charge transfer path is formed within the neck of the single nanoparticle. When this charge transfer path continues to shrink, the CTP mode gradually shifts

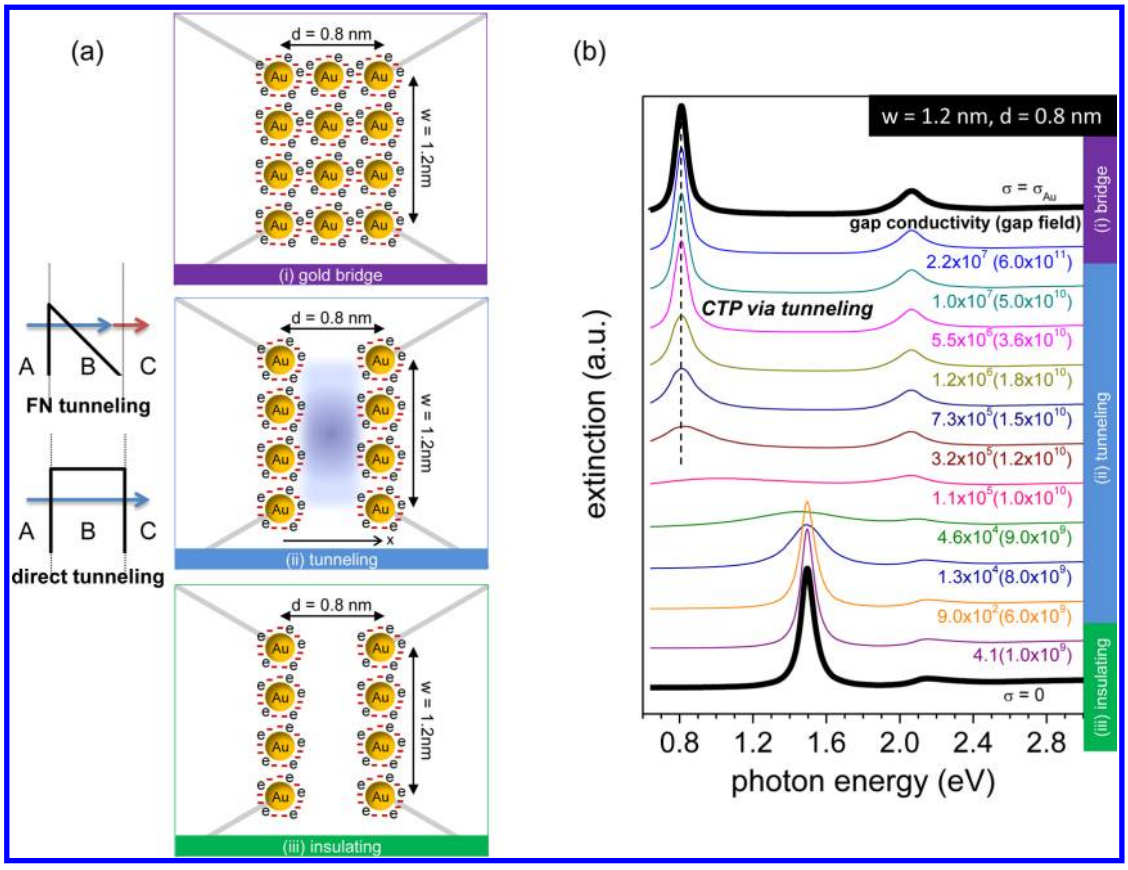

Figure 2. Systematic studies on CTPs in the transition region, from an atomic scale conductive gold bridge to an insulating empty space. (a) Schematics of the three different regions: (i) conductive gold—the charge transfer path is made up of gold atoms with many free electrons surrounding; (ii) conductive gap—the charge transfer path is filled with tunneling electrons, for which the two tunneling mechanisms are presented schematically; (iii) insulating gap—the charge transfer path is empty. (b) The simulated extinction spectra for the three regions for a range of possible path conductivities: (i) gold bridge conductivity $\sigma_{Au} = 4.55 \times 10^7$ S/m, (ii) gap conductivity due to tunneling electrons σ_{gap} (S/m), which is gap field F (V/m) dependent, and (iii) zero conductivity for an insulating gap.

toward a lower energy, and a few higher-order modes[8] appear, for example, hybridized dipolar modes and hybridized quadrupolar modes. Eventually when a gap opens, the CTP mode disappears (Figure 1a bottom). The same phenomenon has indeed been observed experimentally,[8] where a series of bowtie structures were fabricated and characterized by their electron energy-loss spectroscopy (EELS) spectra as shown in Figure 1c. Details of fabrication[17−19] and characterization[20−22] can be found in the Methods section. Both simulations (Figure 1a,b) and experiments (Figure 1c,d) suggest that a CTP should involve oscillating electric charges transferring across the nanostructure. As long as there is a path for transferring charges, a CTP can be obtained.[16] We refer to the CTP shown in Figure 1 as a CTP *via* bridge because its charge transfer path is in the form of a conductive bridge made up of gold atoms. However, from the narrowest 3 nm bridge to the 0.5 nm gap, as shown in Figure 1c bottom, there is an abrupt disappearance of the CTP mode. This abrupt transition region may generate many questions. How does the CTP resonance evolve gradually? At which point does it disappear? What is the underlying mechanism? To answer these questions, a quantum mechanical model is required that takes into account tunneling effects.

Charge Transfer *via* Fowler−Nordheim Tunneling. The classical results presented in Figure 1a show an abrupt termination of the charge transfer when the last layer of connecting atoms is taken out, forming a 0.8 nm gap which is assumed insulating, as schematically shown in Figure 2a. However, this assumption is inaccurate, because electron tunneling may occur in a subnanometer gap, which would make the gap conductive. Therefore a quantum mechanical model to account for the electron tunneling is required. Fundamentally, there are two types of tunneling: direct tunneling and Fowler−Nordheim (FN) tunneling. Direct tunneling is significant for small gaps while FN tunneling dominates if a high electric field is present in the gap. A typical A/B/C structure is considered as shown in (ii) of Figure 2a. For direct tunneling, the electrons from A directly tunnel through the square barrier to C; whereas for FN tunneling, the electrons from A tunnel through the triangular barrier to B and then transport to C. Whenever the FN tunneling occurs, electrons continuously exist in B,

which is commonly termed as "space charge". Thus the charge transfer *via* FN tunneling can also be termed as charge transfer *via* space charge. Here the A/B/C structure we study is gold/vacuum-gap/gold.

To quantitatively describe the tunneling electrons in the gap, we start with the classical Drude model, which is also the microscopic view of Ohm's law:[23] $\sigma = ne^2\tau/m$, where the motion of the free electrons is considered against a background of positive ion cores. The material's conductivity σ is determined by the electron's number density n, charge e, mass m, and mean free time between collisions τ. For a gold bridge, the number density of free electrons $n_{Au} = 5.9 \times 10^{28}$ m^{-3} is fixed,[23] which is related to the number of atoms per unit volume (i.e., Avogadro's number $\times$ density/atomic mass). To calculate the gap conductivity due to the tunneling electrons, n_{Au} is replaced with the term n_{gap} (tunneling electron density in the gap) to represent the number of electrons that tunnel through the barrier. It is worth mentioning that in calculating n_{gap} we have taken into account the Coulomb interaction and the exchange-correlation interaction between electrons based on the Kohn−Sham density function theory.[24,25] The tunneling barrier can be overcome by either increasing the electric field in the gap, or by reducing the gap length to the deep subnanometer regime to make use of the image charge screening effect.

A numerical model is developed here to calculate the tunneling electron density n_{gap} or the gap conductivity σ_{gap} from a known gap length d and electric field in the gap (or in short the gap field) F. The details of the model are discussed in the Methods section, so here we only outline the major steps. The tunneling barrier at the interface of gold and vacuum is modeled by including the image charge potential energy with the effect of anode screening[26] (depending on the gap length d), the external applied electric field potential energy (equivalent to the gap field F), the space charge $\Phi_{sc}(x)$ and exchange-correlation $\Phi_{xc}(x)$ potential energies due to the transmitted electrons in the gap. Physically, the space charge potential describes the classical Coulomb interaction between electrons, the exchange potential is related to the Pauli Exclusion Principle, and the correlation potential denotes the quantum-mechanical part of the Coulomb interaction between electrons. The two terms $\Phi_{sc}(x)$ and $\Phi_{xc}(x)$ were calculated self-consistently between (a) calculating the emitted current density J_{emit} from the tunneling barrier, and (b) calculating $\Phi_{sc}(x)$ and $\Phi_{xc}(x)$ from J_{emit} by the Schrödinger−Poisson approach[12,14,24] to account for the quantum dynamics. For such a complicated tunneling barrier problem, the Miller−Good approximation[27,28] is used to give approximate solutions to the time-independent Schrödinger equation. This approximation is a generalization of the ordinary WKB method, which is a procedure in mathematical physics for finding approximate solutions to linear partial differential equations with spatially varying coefficients. In this way, it is possible to obtain the complete profile of tunneling barrier for any given electron emitter, gap length (d), and gap field (F). From the known barrier profile, the tunneling electron density in a quantum tunneling nanogap can be calculated.

Knowing the tunneling electron density and hence the finite gap conductivity, now we are able to study the CTP *via* tunneling in a similar way as the classical approach that we used for CTP *via* a conductive bridge, by simply substituting the conductivity of the bridge with the value of σ_{gap} and using $\varepsilon(\omega) = 1 + i(\sigma/(\omega\varepsilon_o))$ to obtain the optical response.[5,16] This method is referred to as a quantum-corrected model (QCM),[5] which is a practical approach to study the optical response of large coupled plasmonic systems that include quantum effects. Despite its simplicity, the limitations of our model should be noted. First, QCM only treats the junction between the two nanoparticles quantum-mechanically, whereas the two nanoparticles are still modeled classically using the conventional dielectric function. This simplification disregards the nonlinear optical response from the two nanoparticles at high-field conditions. In this sense, the full quantum mechanical model[4] would be an ideal approach, but is practically limited to only model a small plasmonic system consisting of a few thousand conduction electrons. In addition, it should be noted that within the QCM, a simplified WKB approximation solving the one-dimensional Schrödinger equation was used to solve the tunneling problem in the junction. As compared to a full quantum-mechanical calculation to model the junction, the WKB approximation may underestimate the tunneling events and cause quantitative errors when it comes to derive an exact gap length that trigger out the quantum regime, especially at weak-field conditions.[9] However, these approximations do not affect the results of the present analysis, as it allows us to express a "quantum" conductivity that depends not only on the gap lengths but also on the intensity of the incoming fields. On the basis of this dependence of the field intensity, the field necessary to produce tunneling (and therefore CTP) is established at different gap lengths.

As an example, a nanoprism pair with a 0.8 nm long and 1.2 nm wide gap (Figure 2a) was studied. The extinction spectra in Figure 2b were simulated for various gap conductivities, showing a clear CTP mode when the gap conductivity is above 1.145×10^5 S/m (gold has conductivity of $\sigma_{Au} = 4.55 \times 10^7$ S/m). This CTP mode shown in Figure 2b is the CTP *via* FN tunneling. It should be noted that for the studied 0.8 nm gap length, it is possible to extract and accumulate enough electrons (1.485×10^{26}/m^3) in the space charge region to sustain a CTP, only if the field inside the gap is as large as 10^{10} V/m. Assuming the plasmonic field enhancement in the gap is 20$\times$ in this nonlinear strong-field

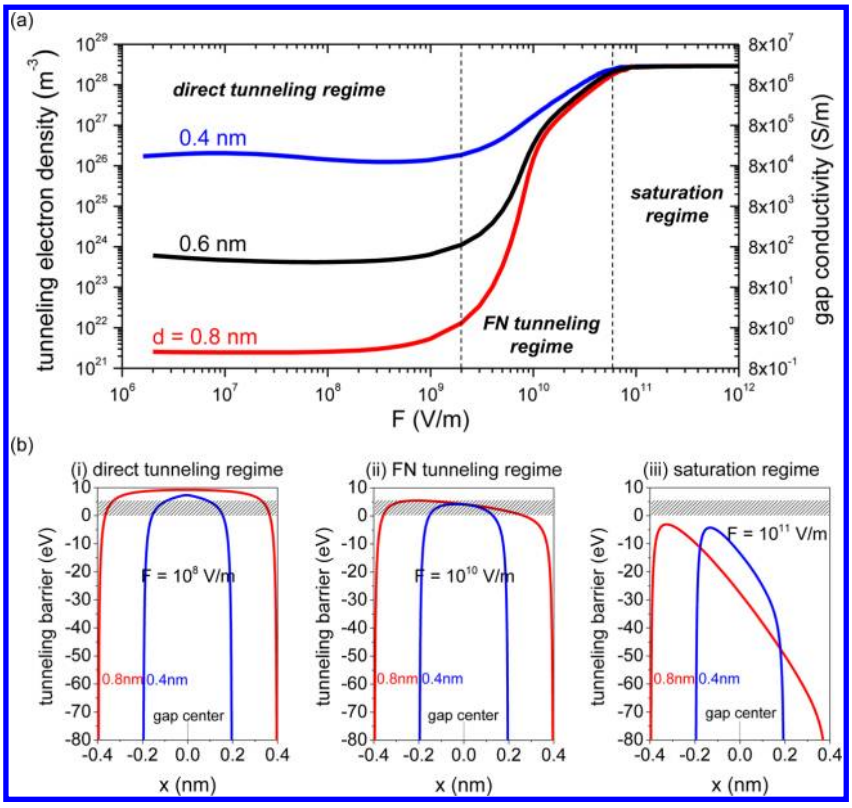

Figure 3. Systematic studies on gap conductivity which is dependent on the gap length and gap field. (a) The calculated tunneling electron density and gap conductivity as a function of the gap field for the gap lengths 0.8, 0.6, and 0.4 nm, where three regimes are identified: direct tunneling, FN tunneling, and saturation. (b) The modeled tunneling barrier profiles inside the gap for the three regimes. The shaded areas in panel b represent the energy levels of the source electrons.

regime for a laser pulse illumination,[4] the excitation of a 10^{10} V/m plasmon-enhanced field requires an incident optical field of 5×10^8 V/m or an incident optical power of 3×10^{10} W/cm^2. For relatively weak plasmonic fields in the gap (*e.g.*, 10^8 V/m), there is still FN tunneling and space charge, but it is simply not dense (2.556×10^{21}/m^3) or conductive (1.972 S/m) enough to sustain the CTP resonant mode. This is one possible reason to explain why we did not observe CTP mode in our previous measurements on the nanoprism pair with the 0.5 nm gap as shown in Figure 1c. In the EELS experiments, a beam of fast electrons is used to excite the plasmons and only one plasmon is excited at a time. As such, we could estimate the fields that would form when a single plasmon is excited in the structures. If we approximate that most of the energy of the plasmon is going to be concentrated within a cubic volume (V_{cube}) near the gap area, then we can use the equation $^1/_2\varepsilon_0|F|^2V_{cube}$ = plasmon energy to calculate the resulting plasmonic field F. Assume that the plasmon has an energy of 2 eV, and the electric fields are confined within a $5 \times 5 \times 5$ nm^3 volume, then the electric field strength of a single plasmon in the gap area is roughly 7.6×10^8 V/m, which is far from the field required for FN tunneling induced CTP (10^{10} V/m).

Excitation Mechanisms. To understand the mechanisms behind the CTP *via* tunneling, we have carefully analyzed the quantum tunneling process under various scenarios. As shown in Figure 3a, the calculated tunneling electron density and gap conductivity are plotted as a function of the electric field in the gap for gap lengths 0.8, 0.6, and 0.4 nm. Three regimes are identified: direct tunneling, FN tunneling, and saturation. For each of the three regimes, the tunneling barrier energy-space profile is shown in Figure 3b.

In the direct tunneling regime, when the external electric field is small, the tunneling barrier is dominated by the image charge potential. In this regime, the gap conductivity mainly depends on the gap length as shown in Figure 3a. When the gap is small, electrons could more easily tunnel through the narrower barrier as shown in Figure 3b(i), the increased tunneling probability increases the tunneling electron density (and gap conductivity). With the gap of 0.4 nm, σ_{gap} is at least on the order of 10^5 S/m, large enough to support the CTP even at weak electric fields. This is the regime studied in the literature so far.[3] However in this direct tunneling regime, the larger 0.8 nm gap cannot support the charge transfer because the tunneling barrier width is too wide.

For such larger gaps, the electric field potential can be increased to induce the FN tunneling, where the tunneling barrier is brought down and narrowed as shown in Figure 3b(ii). With such a rounded triangular

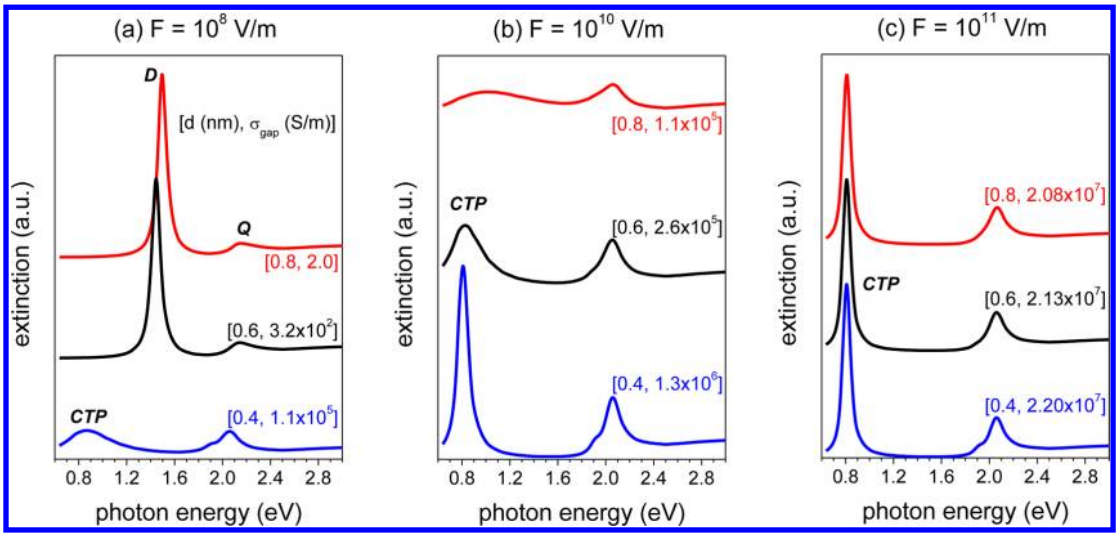

Figure 4. Simulated extinction spectra for the various combinations of gap fields and gap lengths, where different gap conductivities are present. At weak-field condition shown in panel a, the 0.6 and 0.8 nm gap lengths do not support the charge transfer plasmon (CTP) mode, instead the higher-order modes such as a hybridized dipolar (D) mode and a hybridized quadrupolar (Q) mode[8] are shown around 1.5 and 2.1 eV, respectively.

tunneling barrier, electrons overcome the barrier *via* FN tunneling. In the FN tunneling regime, tunneling electron density and gap conductivity are very sensitive to the electric field, and the slope is rather steep as shown in Figure 3a. This steep slope suggests a very interesting feature of CTP *via* FN tunneling, that is, the tunable gap conductivity by the external electric fields (or the intensity of the external irradiation). As the electric fields in the gap varies by 2 orders of magnitude (from 10^9 to 10^{11} V/m), the gap conductivity changes by 7 orders of magnitude (from 1 to 10^7 S/m). This wide range of gap conductivities makes the gap mimic an insulating material or a conductive material, purely dependent on the strength of applied electric fields.

As the field further increases, the barriers are lowered to such a level that all the tunneling electrons are above the barrier as shown in Figure 3b(iii) and are all perfectly transmitted. This is the saturation regime where all the supplied electrons have tunneled through, and the resulting gap conductivity is sufficiently large (>10^7 S/m) to support the CTP for all the gap lengths studied. In this saturation regime, gap conductivity is independent of either gap lengths or electric fields as clearly shown in Figure 3a. Instead it is only limited by the number of supplied electrons from gold nanoparticles. In this sense, the saturation regime represents the "on" state of the CTP mode. However, attention should be paid that further increasing the field beyond the saturation regime may trigger the optical field ionization process, which is not taken into account in our model.

As inferred from Figure 3, there are two approaches to overcome the tunneling barrier to achieve the charge transfer. The first is to make use of image charges screening for direct tunneling, which can be realized in an extremely short gap, for example, 0.4 nm. The second is to use field emission phenomena (*i.e.*, the FN tunneling), which relies on a strong field inside the gap. In contrast to the first approach where everything is fixed after the fabrication, the second one benefits from the freedom of external tunability. To give a more intuitive picture of the charge transfer plasmon resonances, Figure 4 shows the simulated extinction spectra for various combinations of gap length (d) and gap field (F) by putting the calculated σ_{gap} into the optical simulation. With 0.4 nm gap length, the CTP mode always appears as shown in Figure 4 (blue curves): 4a is *via* direct tunneling, and 4b is *via* both direct and FN tunneling. With larger subnanometer gaps like 0.6 and 0.8 nm, applying gap fields on the order of 10^{10} or 10^{11} V/m (Figure 4b,c) could excite the CTP mode. It is clear that the spectral shape of the CTP mode strongly depends on the external fields for each gap length. For example, for the 0.6 nm gap (black curves in Figure 4), the CTP mode is turned off by the 10^8 V/m gap field. The 10^{10} V/m gap field excites a broad and low peak, but the 10^{11} V/m gap field results in a sharp and high peak. The strength of the external field indeed tunes the CTP mode shape.

Energy, Amplitude, Quality-Factor. The most distinctive feature of charge transfer *via* tunneling is the tunable conductivity of the conductive gap. This is different from the CTP *via* a bridge where the conductivity of the gold bridge is fixed (only the bridge size matters as shown in Figure 5b). This tunable conductivity in turn affects the characteristics of the CTP mode. As shown in Figure 5a, for the CTP *via* tunneling, the gap conductivity mainly influences the strength of the CTP, but not the resonant energy. The decreased conductivity strongly lowers and broadens the CTP resonance. In other words, the quality factor (Q-factor) of the CTP, defined as the ratio of the CTP's resonant frequency to its line-width, is strongly degraded by the reduced conductivity. The calculated Q-factors, together with the resonant energies

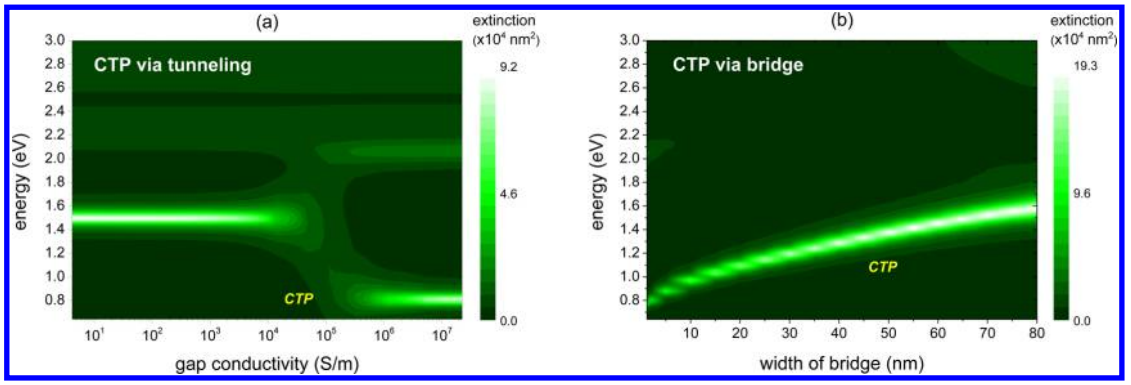

Figure 5. A comparison between the two types of charge transfer plasmon resonances: (a) CTP *via* tunneling and (b) CTP *via* conduction. Here the color bars are the extinction cross sections (nm^2) which represent the strength of the plasmonic resonances.

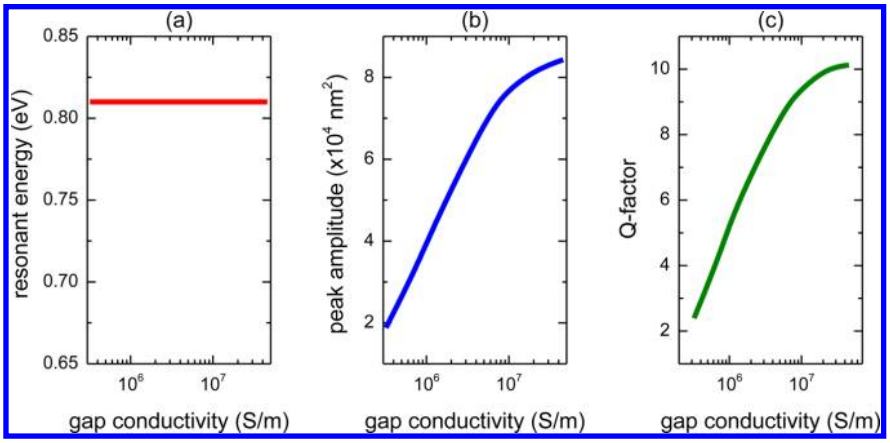

Figure 6. The dependences of the resonant energies, peak amplitudes, and quality factors of the charge transfer plasmons on gap conductivities.

and peak amplitudes, are shown in Figure 6, implying that CTP oscillations dampen out quickly as the gap conductivity decreases. In short, the external-field (or external-irradiation) tunable gap conductivity will result in charge transfer oscillations at the same resonant energies but with variable amplitudes and damping rates. This property of CTP *via* tunneling may enable its applications in the field of high speed switches and modulators.

CONCLUSIONS

In summary, we have investigated charge transfer in subnanometer gaps between nearly touching nanoprisms using a WKB-type approximation to solve the quantum tunneling problem, within the framework of a quantum-corrected model (QCM). Charge transfer plasmons (CTPs) *via* direct or Fowler-Nordheim (FN) tunneling are predicted between two nearly touching nanoprisms. When the gap is ~0.4 nm, merely the intrinsic image charge potential energy is able to extract and accumulate enough electrons to support the CTP. As the gap increases, an external optical field can be utilized to maintain the minimum conductivity of 1.145×10^5 S/m in order to support the CTP, which is based on the FN tunneling mechanism. For instance, a plasmonic gap field of 10^{10} V/m (or an incident power of 3×10^{10} W/cm^2) is needed when the gap length is 0.8 nm. This required threshold could be the reason that CTP was not observed in our fabricated nanoprism pairs with a 0.5 nm gap. Furthermore, CTP *via* FN tunneling is a damped charge transfer plasmonic oscillation process. Its strength and damping rate can be controlled externally by changing the incident light intensity (and hence the electric field in the gap), as light illumination controls the tunneling electron density in the gap and thus the gap conductivity. The mechanism of turning on and off the charge transfer by external optical means lays the foundation for the development of novel quantum devices.

METHODS

Quantum Calculations. A quantum mechanical model is used to numerically calculate the tunneling electron density in the gap of two closely spaced nanoparticles, where the tunneling is driven by the enhanced optical electric fields. The assumptions we made include the following. First, the time-dependent tunneling problem is simplified to a time-independent problem, i.e. the time-independent Schrödinger equation needs to be solved. This is justified as the tunneling time of an electron is typically less than 1 fs,[29−31] which is much shorter than the

period of optical fields – an optical energy of 0.4 eV corresponds to a period of 10 fs. In other words, we have assumed that the electrons see a constant barrier within the subfemtosecond transit time. This assumption will be invalid if the tunneling of electrons is slower than the variation of the driven optical field, and then the time-dependent electron tunneling dynamics must be considered. The second assumption we made is that the gap between the two nanoparticles is much smaller than their face-to-face surface area, therefore the tunneling process is simplified to a one-dimensional (1D) problem along the interparticle axis x.

With the above two assumptions justified, we proceed to solve the time-independent Schrödinger equation for an electron in one dimension:

$$-\frac{\hbar^2}{2m}\frac{d^2\psi(x)}{dx^2}+\Phi(x)\psi(x) = E_0\psi(x) \quad (1)$$

where $\hbar$ is the reduced Planck's constant, m is the electron's mass, x represents the distance measured in the direction of motion of the electron, $\psi(x)$ is the Schrödinger wave function, $\Phi(x)$ is the potential energy of the electron, and E_0 is the energy of the electron that is associated with motion in the x-axis. The potential energy of electron or the tunneling barrier $\Phi(x)$ is modeled by including all the necessary terms as follows:[12,14]

$$\Phi(x) = E_F+\Phi_B+\Phi_{im}(x)+\Phi_v(x)+\Phi_{sc}(x)+\Phi_{xc}(x) \quad (2)$$

which are (i) the Fermi energy level E_F and work function Φ_B of the electron emitter, gold (E_F = 5.53 eV and Φ_B = 5.1 eV);[23] (ii) the image charge potential energy including the effect of anode screening[26] $\Phi_{im}(x) = -[e^2/(16\pi\varepsilon_0 x) + e^2/(8\pi\varepsilon_0)\sum_{\alpha=1}^{\infty}(\alpha d/(\alpha^2 d^2 - x^2) - 1/(\alpha d))]$, where α is a mathematical term for doing the integration, e is the electron's charge, ε_0 is the vacuum permittivity, and d is the gap length; (iii) the external applied electric field potential energy $\Phi_v(x) = -eFx$ where F is the electric field in the gap; (iv) the space charge $\Phi_{sc}(x)$ and exchange-correlation $\Phi_{xc}(x)$ potential energies due to the transmitted electrons in the gap, which need to be self-consistently calculated, together with the emitted current density J_{emit}, as shown in the following two steps.

First, to calculate J_{emit} for a known tunneling barrier $\Phi(x)$, we need to do a numerical integration over all the electrons' energy levels:

$$J_{emit} = e\int_{-\infty}^{+\infty} N(E_x)\,D(E_x)\,dE_x \quad (3)$$

where $N(E_x)\,dE_x$ is the total number of electrons with normal energy between E_x and $E_x + dE_x$ impinging on the surface barrier across a unit area per unit time. From free-electron theory of metal,[32] $N(E_x)\,dE_x = (mk_BT)/(2\pi^2\hbar^3)\ln[1+\exp(-(E_x-E_F)/(k_BT))]$ where k_B is the Boltzmann constant, T is the temperature, and E_F is the Fermi level of the emitter. Each of these electrons has a probability $D(E_x)$ to transmit through the surface potential barrier $\Phi(x)$ that is given by eq 2 where there are two roots of $E_x - \Phi(x) = 0$: x_1 and x_2. This transmission coefficient $D(E_x)$ is approximated by an analytic expression developed by Miller and Good (which is a generalization of the ordinary WKB method):[27,28]

$$D(E_x) = \frac{1}{1+\exp[\Lambda(E_x)]} \quad \text{and}$$

$$\Lambda(E_x) = -\frac{2}{\hbar}\int_{x_1}^{x_2}\sqrt{2m[\Phi(x)-E_x]}\,dx \quad (4)$$

where a linear expansion of $\Lambda(E_x)$ is typically required through the barrier maximum.[28]

Second, to calculate $\Phi_{sc}(x)$ and $\Phi_{xc}(x)$ from J_{emit} in a nanogap, we use the mean field theory[33] for electrons in a one-dimensional potential energy barrier $\Phi(x) = -eV_{sc}(x) - eV_v(x) + \Phi_{xc}(x)$, where the 1D time-independent Schrödinger equation and the Poisson equation (with emitted electron density $n = \psi\psi^*$) are[14]

$$-\frac{\hbar^2}{2m}\frac{d^2\psi}{dx^2} = (E_0+eV_{sc}+eV_v-\Phi_{xc})\psi \quad (5)$$

$$\frac{d^2V_{sc}}{dx^2} = \frac{e\psi\psi^*}{\varepsilon_0} \quad (6)$$

where $\psi(x)$ is the complex electron wave function, E_0 is the electron emission energy, V_{sc} is the space charge potential, $V_v = Fx$ is the applied electric potential, $\Phi_{xc} = \bar{\Phi}_{xc} \times E_H$ is the electron exchange-correlation potential energy with E_H being the Hartree energy. The dimensionless $\bar{\Phi}_{xc}$ is calculated by Kohn–Sham density functional theory (DFT):[25]

$$\bar{\Phi}_{xc} = \epsilon_{xc} - \frac{r_s}{3}\frac{d\epsilon_{xc}}{dr_s} \quad (7)$$

where r_s is the local Seitz radius $[4\pi n(r_s a_0)^3/3 = 1]$ in terms of the Bohr radius a_0. The exchange-correlation energy ϵ_{xc} is the sum of the exchange energy ϵ_x[34] and correlation energy ϵ_c[35] of each electron for a uniform electron gas of density n under the Kohn–Sham local density approximation (LDA). They are

$$\epsilon_x = -\frac{3}{4}\left(\frac{3}{2\pi}\right)^{2/3}\frac{1}{r_s} \quad (8)$$

$$\epsilon_c = -2A(1+a_1r_s)\ln\left[1+\frac{1/2A}{\kappa}\right] \quad (9)$$

where $\kappa = b_1(r_s)^{1/2} + b_2r_s + b_3r_s^{3/2} + b_4r_s^{c+1}$ and c, A, a_1, b_1, b_2, b_3, and b_4 are parametrized constants obtained using the random phase approximation.[35]

The complex wave function $\psi(x)$ can be represented in terms of the nondimensional wave amplitude $q(\bar{x})$ and phase $\theta(\bar{x})$, both assumed real and $\bar{x} = x/d$: $\psi(x) = (n_0)^{1/2}q(\bar{x})\,e^{i\theta(\bar{x})}$, with the density scale $n_0 = (2\varepsilon_0V_g)/(3ed^2)$ and $V_g = Fd$. The charge conservation requires that the current density $J_{emit} = e(i\hbar/(2m))(\psi\psi^{*\prime} - \psi^*\psi')$ be constant for all x, where the prime denotes a derivative with respect to x. Deriving from the definition of J_{emit}, we will have $\theta'(\bar{x}) = {}^2/_3\mu\lambda[q(\bar{x})]^{-2}$, where μ and λ are, respectively, the normalized current density and gap length. More specifically, $\lambda = d/\lambda_0$ is the normalized gap length with respect to the electron de Broglie wavelength: $\lambda_0 = \hbar/(2emV_g)^{1/2}$, and $\mu = J_{emit}/J_{CL}$ is the normalized electron current density with respect to the classical Child–Langmuir current density $J_{CL} = (4\varepsilon_0/9)(2e/m)^{1/2}(V_g^{3/2}/d^2)$. By taking the precise expression of $\psi(x)$ into eqs 5 and 6, we are able to obtain the normalized 1D time-independent Schrödinger equation and the Poisson equation:[24]

$$q'' + \lambda^2\left(\phi_{sc}+\bar{x}-\phi_{xc}-\frac{4}{9}\frac{\mu^2}{q^4}\right)q = 0 \quad (10)$$

$$\phi_{sc}'' = \frac{2}{3}q^2 \quad (11)$$

where q''(and ϕ_{sc}'') denote the second derivative of q (and ϕ_{sc}) with respect to $\bar{x}$, and $\phi_{sc} = eV_{sc}/eV_g$ (and $\phi_{xc} = \Phi_{xc}/eV_g$) is the normalized space charge (and exchange-correlation) potential energy. The boundary conditions for eqs 10 and 11 are $\phi_{sc}(0) = 0$, $\phi_{sc}(1) = 0$, $q(1) = (2\mu/3)^{1/2}$, and $q'(1) = 0$. With these boundary conditions, we can determine the profile of wave amplitude $q(\bar{x})$, space charge potential energy $\phi_{sc}(\bar{x})$, and exchange-correlation potential energy $\phi_{xc}(\bar{x})$ for any value of injected current density μ, at given gap length d and gap voltage $V_g = Fd$.

By solving eqs 3, 10, and 11 shown above iteratively, we are able to obtain the numerically converged results of the complete profile of $\Phi(x)$ for any given electron emitter (E_F, Φ_B), gap length (d), and electric field in the gap (F). From here, the number density of emitted electrons (m^{-3}) in a quantum tunneling nanogap can be calculated by

$$n_{gap} = \int_{-\infty}^{+\infty}\frac{N(E_x)\,D(E_x)}{\sqrt{2E_x/m}}\,dE_x \quad (12)$$

where $N(E_x)\,D(E_x)$ is the number of emitted electrons across a unit area per unit time, and $(2E_x/m)^{1/2}$ is the velocity of electrons at energy level E_x.

Nanostructure Fabrications. The gold nanoprisms were fabricated onto 30-nm-thick silicon nitride (SiN_x) membranes using electron-beam lithography (EBL) combined with a lift-off process.[17] In detail, PMMA resist (950 K molecular weight, 1.67% in anisole) from MicroChem Corp. was spin-coated at 4 k rpm to

be ~65 nm thick on the SiN_x substrate. After spin-coating, the substrates were baked on a hot plate at 180 °C for 90 s. EBL was done with an Elionix ELS-7000 system with an accelerating voltage of 100 kV and a beam current of 50 pA. We used a layout that had nanoprism pairs with gaps that were nominally designed to range from 14 to 0 nm in steps of 2 nm. An optimized dose was used to obtain the structures we designed for the measurements. After exposure, the samples were developed with 1: 3 MIBK:IPA developer at low temperature (0 °C) for 30 s and then were directly blown dry with a steady stream of N_2. Metal deposition was performed using an electron-beam evaporator (Explorer Coating System, Denton Vacuum). A 15 nm Au layer was deposited with 1 nm Cr adhesion layer. The thickness of Cr adhesion layer was intentionally minimized to reduce its damping effect on plasmon resonance. The temperature of the sample chamber was kept at 20 °C during the entire evaporation process, with the sample holder rotating at a rate of 50 rpm to ensure the uniformity of deposition. Lift-off was done in *N*-methylpyrrolidone (NMP) at an elevated temperature of 70 °C. To study the effect of decreasing bridge width, we kept the total length of the nanoprism pair the same but varied only the width of the conductive bridge.

EELS Experiments. Electron energy-loss spectroscopy was performed in STEM mode using an FEI Titan TEM with Schottky electron source, operated at 80 kV, using a convergence semiangle of 13 mrad. A Wien-type monochromator dispersed the electron beam in energy, and a narrow energy-selecting slit formed a monochrome electron beam with typical full-width at half-maximum values of 60 meV and full width at 1/1000 of maximum values around 0.7 eV. The electron beam was focused to a probe with a diameter less than 1 nm. Attached to the TEM was a Gatan Tridiem ER EELS detector used for EELS mapping and spectroscopy. Applying a 7 mrad collection semiangle, EELS data were acquired with a modified binned gain averaging routine.[20] In short, individual spectra were acquired in 40 ms, using 16 times on-chip binning. The detector channel-to-channel gain variation was averaged out by constantly changing the readout location and correcting for these shifts after completing the EELS acquisition. A high-quality dark reference was acquired separately, and used for postacquisition dark signal correction. Spectra were normalized by giving the maximum of the spectra (the top of the zero-loss peak) unit value. All spectra were acquired by placing the STEM probe 1−2 nm off the metal surfaces. The quasi-elastic background signal was corrected for by fitting and subtracting a high-quality premeasured background spectrum. Typical signal-to-noise ratios of 1×10^4 for individual spectra were obtained.

Conflict of Interest: The authors declare no competing financial interest.

Acknowledgment. L.W., P.B., and E.P.L. gratefully acknowledge the financial support by Agency for Science and Technology Research (A*STAR) Singapore with Thematic Strategic Research Programme (TSRP) Grants: iNPBi—LSPR POC for Clinical Screening and Medical Diagnostics no. 102152 0014, and Metamaterials—Nanoplasmonics no. 0921540098. The authors would like to acknowledge the financial support by National Research Foundation Singapore under its Competitive Research Programme (CRP Award no. NRF-CRP 8-2011-07). H.D. gratefully acknowledges the partial sponsorship from NSFC (Grant Nos. 11274107 and 61204109).

REFERENCES AND NOTES

1. Romero, I.; Aizpurua, J.; Bryant, G. W.; De Abajo, F. J. G. Plasmons in Nearly-Touching Metallic Nanoparticles: Singular Response in the Limit of Touching Dimers. *Opt. Express* **2006**, *14*, 9988–9999.
2. Lassiter, J. B.; Aizpurua, J.; Hernandez, L. I.; Brandl, D. W.; Romero, I.; Lal, S.; Hafner, J. H.; Nordlander, P.; Halas, N. J. Close Encounters between Two Nanoshells. *Nano Lett.* **2008**, *8*, 1212–1218.
3. Zuloaga, J.; Prodan, E.; Nordlander, P. Quantum Description of the Plasmon Resonances of a Nanoparticle Dimer. *Nano Lett.* **2009**, *9*, 887–891.
4. Marinica, D. C.; Kazansky, A. K.; Nordlander, P.; Aizpurua, J.; Borisov, A. G. Quantum Plasmonics: Nonlinear Effects in the Field Enhancement of a Plasmonic Nanoparticle Dimer. *Nano Lett.* **2012**, *12*, 1333–1339.
5. Esteban, R.; Borisov, A. G.; Nordlander, P.; Aizpurua, J. Bridging Quantum and Classical Plasmonics with a Quantum-Corrected Model. *Nat. Commun.* **2012**, *3*, 825.
6. Atay, T.; Song, J. H.; Nurmikko, A. V. Strongly Interacting Plasmon Nanoparticle Pairs: From Dipole−Dipole Interaction to Conductively Coupled Regime. *Nano Lett.* **2004**, *4*, 1627–1631.
7. Schnell, M.; García-Etxarri, A.; Huber, A. J.; Crozier, K.; Aizpurua, J.; Hillenbrand, R. Controlling the Near-Field Oscillations of Loaded Plasmonic Nanoantennas. *Nat. Photonics* **2009**, *3*, 287–291.
8. Duan, H.; Fernández-Domínguez, A. I.; Bosman, M.; Maier, S. A.; Yang, J. K. W. Nanoplasmonics: Classical Down to the Nanometer Scale. *Nano Lett.* **2012**, *12*, 1683–1689.
9. Savage, K. J.; Hawkeye, M. M.; Esteban, R.; Borisov, A. G.; Aizpurua, J.; Baumberg, J. J. Revealing the Quantum Regime in Tunneling Plasmonics. *Nature* **2012**, *491*, 574–577.
10. Ward, D. R.; Hüser, F.; Pauly, F.; Cuevas, J. C.; Natelson, D. Optical Rectification and Field Enhancement in a Plasmonic Nanogap. *Nat. Nanotechnol.* **2010**, *5*, 732–736.
11. Fursey, G. N. *Field Emission in Vacuum Microelectronics*; Kluwer Academic: New York, 2005.
12. Wu, L.; Ang, L. K.; Koh, W. S. Theory of Shot Noise in High-Current Space-Charge-Limited Field Emission. *Phys. Rev. B* **2008**, *77*, 115351.
13. Wu, L.; Ang, L. K. Non-equilibrium Model of Ultrafast Laser Induced Electron Photo-Field Emission from a DC-Biased Metallic Surface. *Phys. Rev. B* **2008**, *78*, 224112.
14. Wu, L. *Modelling of electron emission: its physics and novel applications*. Ph.D. Thesis, Nanyang Technological University, Singapore, 2009.
15. Child, C. D. Discharge from Hot CaO. *Phys. Rev., Ser. I* **1911**, *32*, 492–511.
16. Pérez-González, O.; Zabala, N.; Borisov, A. G.; Halas, N. J.; Nordlander, P.; Aizpurua, J. Optical Spectroscopy of Conductive Junctions in Plasmonic Cavities. *Nano Lett.* **2010**, *10*, 3090–3095.
17. Koh, A. L.; McComb, D. W.; Maier, S. A.; Low, H. Y.; Yang, J. K. W. Sub-10-nm Patterning of Gold Nanostructures on Silicon-Nitride Membranes for Plasmon Mapping with Electron Energy-Loss Spectroscopy. *J. Vac. Sci. Technol., B* **2010**, *28*, C6O45–C6O49.
18. Koh, A. L.; Fernndez-Domnguez, A. I.; McComb, D. W.; Maier, S. A.; Yang, J. K. W. High-Resolution Mapping of Electron-Beam-Excited Plasmon Modes in Lithographically Defined Gold Nanostructures. *Nano Lett.* **2011**, *11*, 1323–1330.
19. Duan, H. G.; Hu, H. L.; Kumar, K.; Shen, Z. X.; Yang, J. K. W. Direct and Reliable Patterning of Plasmonic Nanostructures with Sub-10-nm Gaps. *ACS Nano* **2011**, *5*, 7593–7600.
20. Bosman, M.; Keast, V. J.; Watanabe, M.; Maaroof, A. I.; Cortie, M. B. Mapping Surface Plasmons at the Nanometer Scale with an Electron Beam. *Nanotechnology* **2007**, *18*, 165505.
21. Bosman, M.; Keast, V. J. Optimizing EELS Acquisition. *Ultramicroscopy* **2008**, *108*, 837–846.
22. Bosman, M.; Anstis, G. R.; Keast, V. J.; Clarke, J. D.; Cortie, M. B. Light Splitting in Nanoporous Gold and Silver. *ACS Nano* **2012**, *6*, 319–326.
23. Ashcroft, N. W.; Mermin, N. D. *Solid State Physics; Saunders*, **1976**.
24. Ang, L. K.; Kwan, T. J. T.; Lau, Y. Y. New Scaling of Child-Langmuir Law in the Quantum Regime. *Phys. Rev. Lett.* **2003**, *91*, 208303.
25. Kohn, W.; Sham, L. J. Self-Consistent Equations Including Exchange and Correlation Effects. *Phys. Rev.* **1965**, *140*, A1133–A1138.
26. Il'chenko, L. G.; Goraychuk, T. V. Role of the Image Forces Potential in the Formation of the Potential Barrier between Closely Spaced Metals. *Surf. Sci.* **2001**, *478*, 169–179.

27. Miller, S. C., Jr.; Good, R. H., Jr. A WKB-type Approximation to the Schrödinger Equation. *Phys. Rev.* **1953**, *91*, 174–179.
28. Jensen, K. L.; Cahay, M. General Thermal-Field Emission Equation. *Appl. Phys. Lett.* **2006**, *88*, 154105.
29. Uiberacker, M.; Uphues, Th.; Schultze, M.; Verhoef, A. J.; Yakovlev, V.; Kling, M. F.; Rauschenberger, J.; Kabachnik, N. M.; Schröder, H.; Lezius, M.; *et al*. Attosecond Real-Time Observation of Electron Tunneling in Atoms. *Nature* **2007**, *446*, 627–632.
30. Nimtz, G. Tunneling Confronts Special Relativity. *Found. Phys.* **2011**, *41*, 1193–1199.
31. Thornber, K. K.; McGill, T. C.; Mead, C. A. The Tunneling Time of an Electron. *J. Appl. Phys.* **1967**, *38*, 2384–2385.
32. Omar, M. Ali. *Elementary Solid State Physics: Principles and Applications*; Addison-Wesley Publishing Company: Reading, MA, 1993.
33. Lau, Y. Y.; Chernin, D.; Colombant, D. G.; Ho, P.-T. Quantum Extension of Child–Langmuir Law. *Phys. Rev. Lett.* **1991**, *66*, 1446–1449.
34. Dirac, P. A. M. Note on Exchange Phenomena in the Thomas Atom. *Proc. Cambridge Philos. Soc.* **1930**, *26*, 376–385.
35. Perdew, J. P.; Wang, Y. Accurate and Simple Analytic Representation of the Electron-Gas Correlation Energy. *Phys. Rev. B* **1992**, *45*, 13244–13249.